Journal of Energy Storage 93 (2024) 112420

Contents lists available at ScienceDirect

Journal of Energy Storage

journal homepage: www.elsevier.com/locate/est

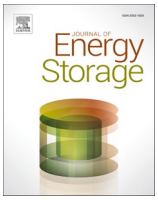

Research papers

Form-stable bitumen/paraffin-wax/polymer binders for energy-efficient building applications

A.A. Cuadri *, C. Delgado-Sánchez, A. Tenorio-Alfonso, P. Partal, F.J. Navarro

Pro²TecS-Chemical Process and Product Technology Research Centre, Department of Chemical Engineering, ETSI, Campus de "El Carmen", Universidad de Huelva, 21071 Huelva, Spain

ARTICLE INFO

Keywords:
Energy-efficient building materials
Thermal energy storage
Phase change materials
Temperature regulation test
Product engineering

ABSTRACT

Novel form-stable bitumen/paraffin-wax/polymer binders were successfully manufactured to be applied as energy-efficient building materials with advanced thermal energy storage and thermoregulation features. These roofing materials are composed of bitumen (B), styrene butadiene styrene copolymer (SBS), and paraffin wax (PW) as phase change material (PCM) for thermal energy storage applications. Systems with a fixed weight ratio B/SBS = 7.33 and PW concentration ranging from 0 to 70 wt% were prepared. Then, thermal stability, microstructure, rheological properties, technological and leakproof performance tests were performed on these binders to assess the optimal compositions. After that, a comprehensive thermal energy storage characterization was conducted on the selected prototypes and, finally, the temperature regulation performance was studied by using simulated solar irradiation. All materials show excellent thermal stability no matter PW concentration used, whereas the rheological properties improve as PW content in blends increases. However, softening temperature requirements, specified by ASTM D8051, limited PW concentration to 30 wt%. Interestingly, no liquid PW leakage from bituminous matrix was found for such a concentration, which has a high heat storage capacity (ca. 60 J/g) and suitable thermal properties (e.g. thermal conductivity and specific heat capacity). As a result, material exhibits a complex solar and thermal behaviour that yields a Latent Heat Thermoregulation Index (LHTI) value greater than for other efficient energy building materials.

1. Introduction

Thermal energy storage (TES) based on latent heat phase change materials (PCMs) is attracting considerable attention for use in the building sector as an advanced approach to energy storage [1–3]. This sector consumes 30 % of the world's total energy, which represents 40 % of the total energy in the EU, and is also responsible for approximately 40 % of the total CO_2 emissions [2]. For this reason, the efforts to develop novel efficient energy building materials based on PCMs have been growing intensively [1,4,5]. To that end, organic paraffin waxes (PWs) are potential PCMs preferred due to their advantages such as large energy density, low supercooling, good chemical and phase change stability, and low cost [6].

Bitumen, a by-product from crude oil distillation, has been widely used in roofing and waterproofing membranes for building applications due to its suitable properties (superior waterproof, adhesive properties, low cost, etc.) [7,8]. In this regard, development of TES materials based on bitumen faces the great challenge of the PCM effective integration to prevent its leakage during the solid-to-liquid transition [6,9]. In addition to that, the high flammability of PCMs in construction and solar energy systems is currently another major concern [10]. Thus, previous research demonstrated that the fire-retardant properties of PCMs can be enhanced by physically blending them with flame retardants, including intumescent flame retardants [11,12], magnesium hydroxide [13], and montmorillonite [14]. As an alternative, chemical modification by phosphorus-containing flame retardants has emerged as an effective strategy to enhance the flame retardancy of PCMs [15,16]. Techniques like PCM encapsulation by a protective shell and the formation of shape-stabilized (or form-stable) PCMs are employed to eliminate the leakage potential [6]. The encapsulation of PCMs is the most mature technology to manufacture PCM/bituminous binders, especially for paving applications [17–20]. However, this approach has some drawbacks that would restrict its industrial applications, including the high cost of the procedure and the daunting task of selecting and developing the appropriate materials for the application [21]. On the other hand, form-stable heat storage materials are manufactured by mixing PCMs with

* Corresponding author.
E-mail address: antonio.cuadri@diq.uhu.es (A.A. Cuadri).

https://doi.org/10.1016/j.est.2024.112420
Received 20 February 2024; Received in revised form 15 April 2024; Accepted 1 June 2024
Available online 6 June 2024

carrier materials (e.g. inorganic porous media and polymers) that confine the flow of PCMs [22]. Inorganic porous materials exhibit a high surface area and excellent thermal stability which make them appropriate carrier materials to produce form-stable PCMs using the vacuum impregnation technology [5]. However, most of inorganic supporting materials such as graphene oxide [23] or carbon nanotubes [24] are expensive and difficult to synthetize. Consequently, these carrier materials are not economical for use in building applications [1]. Polymers like polypropylene [25] or epoxy resin [19] were also used as carrier materials to prepare form-stable PCMs that dampens working temperature of pavements.

With all this in mind, as an alternative to PCM microencapsulation or the use of inorganic porous materials, this work addresses a novel approach to prevent PCM leakage through the development of form-stable TES bituminous materials for building applications. To that end, materials composed by bitumen, styrene butadiene styrene (SBS) triblock copolymer (a polymer typically used in roofing industry) and paraffin wax (acting as PCM) were proposed. In this sense, it is well-known that binary SBS/bitumen blends containing high SBS content (commonly >5–7 wt%) exhibit excellent thermomechanical properties at low and high in-service temperatures, which is ascribed to the creation of a continuous polymer-rich phase throughout the sample [26]. Interestingly, the inclusion of SBS in the ternary blends is expected not only to improve the material thermomechanical response needed to meet with the specifications, but also to hold the maximum amount of paraffin wax without leakage from the created SBS network. Thus, ternary blends at a fixed bitumen/SBS mass ratio (equivalent to the binary 12 wt% SBS/bitumen typically used in roofing applications [27]) were manufactured, and the effects of paraffin wax concentration on microstructure, thermal stability, rheological properties, technological tests and leakproof performance were evaluated. Subsequently, a comprehensive thermal energy storage characterization was conducted on selected ternary binders to evaluate their thermal storage capacity, thermal reliability, thermal conductivity and specific heat capacity. Finally, the temperature regulation performance of these prototypes was studied by subjecting samples to a simulated solar irradiation. The experimental design for this study is illustrated in Fig. 1. The obtained results revealed that ternary bitumen/SBS/paraffin wax binders here proposed are promising form-stable roofing materials for thermal energy storage applications.

2. Experimental

2.1. Materials

A paraffin wax (referred to as PW), supplied by Panreac-AppliChem (Spain), with a melting temperature around 60 °C, was used as PCM. A SBS (styrene butadiene styrene) triblock copolymer containing 31 wt% styrene (trade name C501), provided by Dynasol (Spain), was employed as bitumen modifying agent. A base bitumen (referred to as B), with penetration grade within the range 40/50, was also used.

2.2. Sample preparation

A binary B/SBS blend containing 12 wt% SBS (usual formulation of the roofing industry) was prepared in a Silverson L5 Laboratory mixer, using a general-purpose disintegrating head, at 180 °C with an agitation speed of 3500 rpm for 2 h. Similarly, preparation of ternary B/SBS/PW bituminous blends followed the same processing protocol but including a final PW addition for 15 min (see Fig. 1).

Ternary B/SBS/PW blends were prepared at a fixed B/SBS mass ratio of 7.33 (which corresponds to the reference binary B/SBS sample) and varying the total amount of PW. The nomenclature and composition of the bituminous samples considered in this paper are gathered in Table 1.

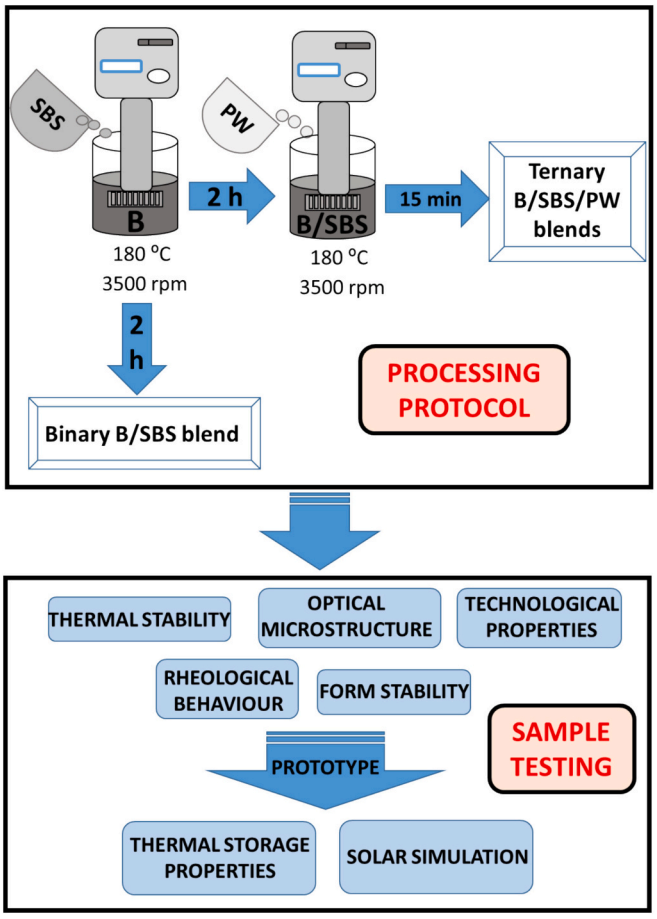

Fig. 1. Experimental design for this study.

Table 1
Nomenclature and composition of the bituminous samples.

Nomenclature	Bitumen (wt%)	SBS (wt%)	B/SBS (wt%/wt%)	Paraffin wax (wt%)
B	100	0	–	0
B/SBS	88.0	12	7.33	0
B/SBS/20	70.4	9.6	7.33	20
B/SBS/30	61.6	8.4	7.33	30
B/SBS/40	52.8	7.2	7.33	40
B/SBS/50	44.0	6.0	7.33	50
B/SBS/60	35.2	4.8	7.33	60
B/SBS/70	26.4	3.6	7.33	70

2.3. Tests and measurements

Rheological properties of samples (oscillatory-shear temperature sweep tests) were performed with a controlled-strain Ares-G2 rheometer (TA Instruments, New Castle, DE, USA). TGA (10 °C·min^{-1}; from 30 to 550 °C) were conducted in a TA Q-50 (TA Instruments, USA). Optical microscopy images were taken by an Olympus BX51 (Japan) microscope coupled to an LTS-350 Heating-Freezing Stage controlled by a Linkam TP94 (Linkam Scientific Instruments, UK). DSC was performed with a Q-250 DSC (TA Instruments, USA). The in-plane thermal conductivity was measured using the non-destructive Transient Hot-Bridge (THB) technique by a THB 100 device from Linseis GmbH (Germany). The temperature regulation tests were carried out by using a Xenon lamp HXF300-T3 (Beijing China Education Au-light Technology Co., Ltd., China).

More detailed information on the characterization can be found in the Supporting Information.

3. Results and discussion

3.1. Binder performance and microstructure

The effect of PW concentration on thermal stability, rheological properties, microstructure, technological tests and leakproof performance of ternary B/SBS/PW binders was initially evaluated.

3.1.1. Thermogravimetric analysis

TGA was used to assess the thermal stability of the ternary binders. Fig. 2 shows the weight loss and its derivative (DTG) for parent components (B, PW and SBS) and their corresponding B/SBS/PW blends.

On the one hand, PW and SBS show the typical one single degradation stage, with their maximum rate located at 318 °C and 546 °C, respectively, and with no char residues observed (Fig. 3A and B). On the other hand, bitumen (B) presents a mass loss process in a wider temperature range composed of two overlapped peaks, with its maximum rate at the same temperature as that noticed for SBS. In addition, a char content of 15 wt%, which is the common response for polycyclic condensed aromatics hydrocarbons compounds [28], was noted in B sample. With regard to B/SBS/PW binders (Fig. 2C and D), the magnitude of their two thermal decomposition stages and the char content are dependent on the blends' composition. Interestingly, at 180 °C, which is a typical temperature used for the manufacture of bitumen-based roofing materials [29], the weight loss is ca. 0.25 wt% for all ternary blends. Therefore, all systems guarantee their thermal stability not only in the temperature range for solar energy collection (< 60 °C) [30,31], but also at the high processing temperatures required in roofing industry [32].

3.1.2. Thermomechanical performance and microstructure

With respect to their thermomechanical performance, it is worth highlighting that the properties required for a roofing material such as low-temperature flexibility and medium/high-temperature structural integrity are directly related to material viscoelastic response. In this sense, Fig. 3 display the evolution of complex modulus |G*| (stiffness and overall resistance to deformation), and loss tangent, tan δ, (inversely proportional to the elasticity of the sample) between −60 and 30 °C, for pristine PW and selected binders. As can be observed, all samples undergo a decrease in |G*| with increasing temperature, exhibiting a predominantly elastic character (tan δ < 1) which is less apparent as temperature rises. However, notable differences among samples can be found that deserve to be analysed. As for pristine PW, |G*| begins to decrease up to −40 °C and, next, undergoes a significant flattening in the slope before decreasing again at ca. 0 °C, leading to almost constant tan δ values in this temperature range. As shown in Fig. 3A, PW presents the highest |G*| value at 30 °C attributed to the large presence of PW crystals (PW presents a crystallinity of 73.7 %, as will be discussed later). Thus, at 25 °C, pristine PW develops a highly interconnected three-dimensional network structure with large needle-like crystals (Fig. 4A). Finally, the observed tan δ peak at −50 °C in Fig. 3B is attributed to the so-called α-relaxation, typically found in polyolefins with a crystallinity above 55 % [33].

With regard to the binary B/SBS sample, similar |G*| values to pristine PW up to −40 °C are observed, but then a continuous decrease with increasing temperature takes place, reaching a |G*| value at 30 °C much lower than PW. In addition, it should be noted that tan δ presents a maximum at ca. -5 °C followed by a decrease up to 10 °C, which indicates a higher sample elasticity at this temperature range. The same finding has been reported for highly SBS modified bitumen at the same testing temperature window [34]. It is well known that binary bitumen/SBS sample with high polymer content (commonly above 5–7 wt%) shows enhanced rheological properties compared to its parent base bitumen, which is ascribed to the creation of a continuous polymer network (polymer-rich phase) throughout the binder. This microstructure is clearly seen for binary B/SBS sample in Fig. 4B, where the SBS-rich phase appears as light red zones and the bitumen-rich one as dark regions.

Interestingly, compared to B/SBS blend, a higher PW content in ternary B/SBS/PW binders leads to materials with: (a) lower |G*| values

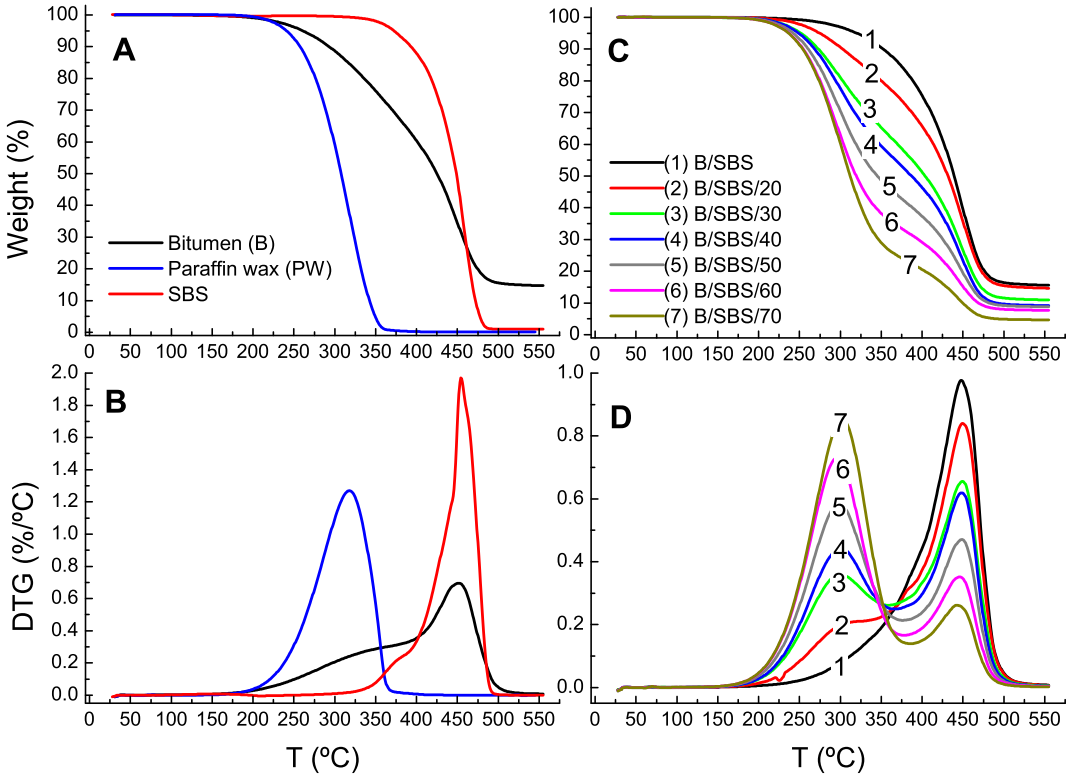

Fig. 2. Weight loss and its derivative (DTG) for parent components (A and B) and their corresponding blends (C and D).

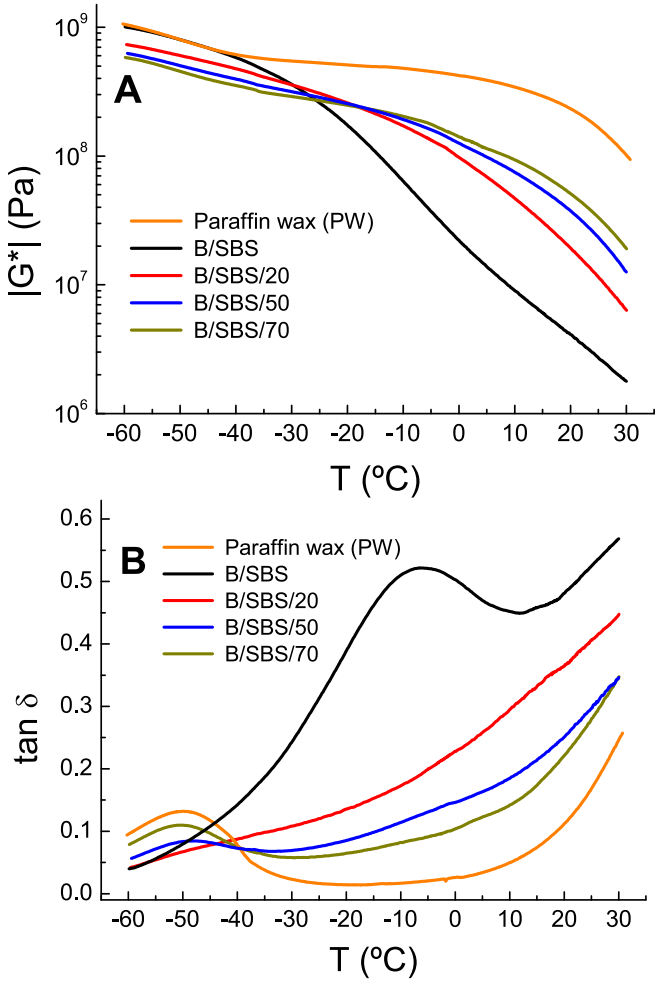

Fig. 3. Evolution of A) complex modulus and B) loss tangent with testing temperature for pristine PW, binary B/SBS binder, and selected B/SBS/PW binders.

at low temperatures (below the glassy region and, thereby, with improved low-temperature flexibility), (b) higher |G*| value at 30 °C (increasing material structural integrity at medium/high temperatures), and (c) lower tan δ values within the interval from −30 to 30 °C (increasing binder elastic properties). The micrographs for these ternary blends may be helpful in explaining these results. Thus, B/SBS/20 binder still displays a continuous SBS-rich phase, as deduced from the micrograph taken without crossed polarizers (Fig. 4C) where PW crystals are not visible. If the same micrograph is taken under crossed polarizers (Fig. 4D), which allow PW crystals to be detected, a significant amount of PW crystals is visible together with the SBS-rich phase. However, it has been reported that paraffin wax and bitumen exhibit a partial miscibility [33], which may alter the colloidal arrangement of bitumen compounds due to the amorphous PW phase (chemically similar to the saturates compounds of bitumen). This fact could be behind the improvement in the low-temperature flexibility for ternary blends, since the greater degree of SBS bitumen modification (and, therefore, the change in rheological properties) is inevitably linked to the higher proportion of light compounds (i.e., saturates) present in the bitumen [26]. For the ternary blends, the higher structural integrity at 30 °C (higher values of |G*|) is clearly associated to the higher presence of PW crystals. Thus, the blend containing 50 wt% PW (Fig. 4E) and, particularly, the system with 70 wt% (Fig. 4F), display a higher proportion of PW crystals, with a more homogeneous distribution throughout the binder, but with smaller, finer, and less developed crystals. The observed higher content of PW crystals in the ternary blends is also corroborated by its α-relaxation noticed in the tan δ peak at −50 °C (Fig. 3B).

3.1.3. Technological characterization

Even though a higher PW content in ternary blends results in an improvement of structural integrity at 30 °C, this property is expected to worsen after the melting process of PW crystals. To explore this, the high temperature performance of ternary blends was evaluated by means of ring and ball softening temperature ($T_{R\&B}$) tests, commonly used in technological characterization of bitumen. Firstly, as seen in Fig. 5A, bitumen modification of base bitumen by 12 wt% SBS produces a significant increase in $T_{R\&B}$ value from 54 °C (for base bitumen) up to 113 °C for B/SBS sample, due to the formation of a continuous polymer network throughout the binder (Fig. 4B). However, with increasing PW content from 20 to 70 %, ternary blends (B/SBS/20 to B/SBS/70) undergo a progressive drop in their $T_{R\&B}$ values from 102 °C up to 77 °C (Fig. 5A). Therefore, binder performance at high temperature is significantly worsened with increased PW content, which would limit its potential application as roofing materials. In fact, the International Standard ASTM D8051 for wax-modified asphaltic products intended for use in roofing applications demands $T_{R\&B}$ values between 99 and 110 °C (striped area in Fig. 5A). As can be seen, ternary blends meet this requirement for PW concentrations up to 30 wt%. As for penetration (P) values at 25 °C (and, thereby, at a testing temperature below PW melting process), all binders match the values established by this Standard (values between 12 and 30 1/10-mm), as deduced from Fig. 5B, with no significant differences among the binders. Therefore, for a fixed B/SBS mass ratio (which corresponds to the reference B/SBS sample), the technological tests specified in ASTM D8051 would limit the maximum PW concentration to 30 wt%.

3.1.4. Leakproof performance

Finally, results derived from leakage test are crucial for these materials. Thus, this test would provide information about the ability of the created SBS network to hold the PW during the melting process and, thereby, about its shape stability. The study was performed by placing a portion of sample in an oven at 80 °C for 1 h, and the corresponding digital photographs after the test are presented in Fig. 6. In addition to that, the mass sample difference before (M_B) and after (M_A) heating can be used to calculate the leak percentage (L) as follows:

$$L = \frac{M_B - M_A}{M_B} \times 100 \quad (1)$$

Interestingly, for ternary binders containing 20 and 30 wt% PW no liquid leakage was detected. Some traces of liquid PW were noticed for B/SBS/40 (L = 0.3 %). However, the PW leakage is clearly visible in B/SBS/50 sample (L = 1.8 %), and becomes massive for binders formulated with 60 wt% PW (L = 19.1 %) and 70 wt% PW (L = 36.9 %). It is important to note that the leaked PW appears darkened, which point outs the partial miscibility between bitumen and PW [33]. In addition, results from the leakage test are in good agreement with the ring and ball softening point. The $T_{R\&B}$ value is related to the collapse of the SBS network, i.e. with the integrity of polymeric structure that below a critical point would not prevent PW leakage. Indeed, ternary blends with $T_{R\&B}$ value higher than 80 °C (temperature used in the leakage test) display much better leakproof performance than that with $T_{R\&B}$ value of 80 °C (B/SBS/60) or 77 °C (B/SBS/70).

In summary, ternary blends containing 20 and 30 wt% PW (i.e., B/SBS/20 and B/SBS/30 binders) have been selected as prototypes for further thermal energy storage characterization, since they present excellent thermal stability; improved rheological properties at low and medium/high temperatures; meet the technological tests established by ASTM D5081; and show excellent leakproof performance.

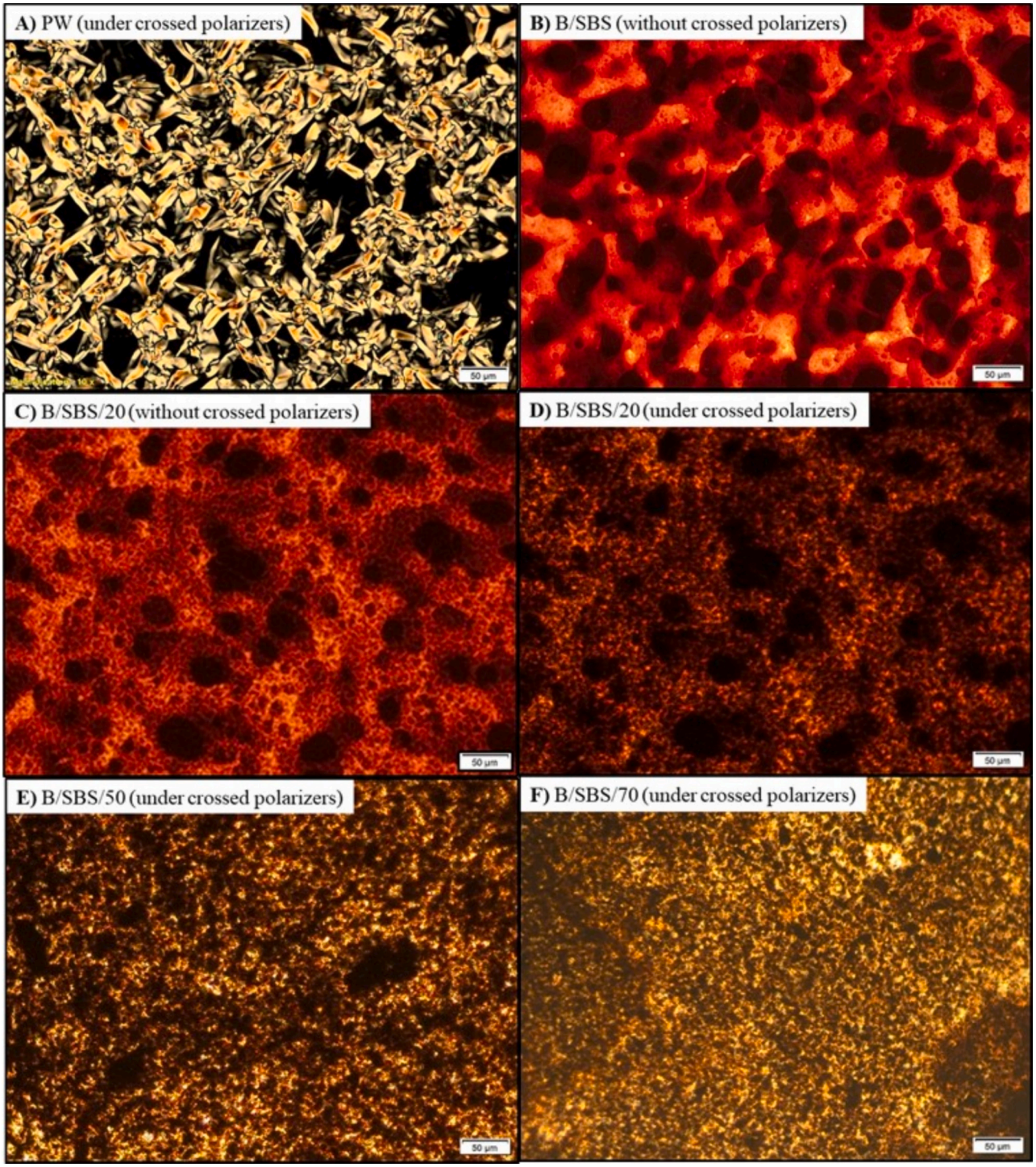

Fig. 4. Micrographs, taken at 25 °C, for pristine PW, binary B/SBS binder, and selected B/SBS/PW binders.

3.2. Thermal energy storage characterization

3.2.1. Thermal storage capacity

The thermal storage capacity of pristine PW and the two selected B/SBS/PW binders was studied by DSC experiments. As observed in Fig. 7A, all DSC scans, after 1 thermal cycle, display wide asymmetric endothermic and exothermic events associated to the melting and crystallization of the crystalline structures. With regard to pristine PW, Table 2 shows its peak temperatures ($T_{m,p}$ and $T_{c,p}$) at 57.9 °C and 56.9 °C for melting and crystallization, respectively; however, these values (and, thereby the onset temperatures, $T_{m,o}$ and $T_{c,o}$) are shifted to lower temperatures as PW concentration in the ternary blends decreases. Although, this effect may have different origins, it is caused by morphological influences due to thermodynamically favourable interactions between the components in the mixture, such as changes in lamellar thickness, degree of crystalline perfection, properties of the amorphous phase surrounding the crystalline phase, thermodynamic behaviour of the mixture, etc. However, as has already been reported for bituminous mixtures [33], this depression of the phase transition point is associated with the formation of crystallites with smaller sizes associated to partial compatibility. Therefore, since the saturates are chemically equivalent to paraffins and, therefore miscible, it is expected

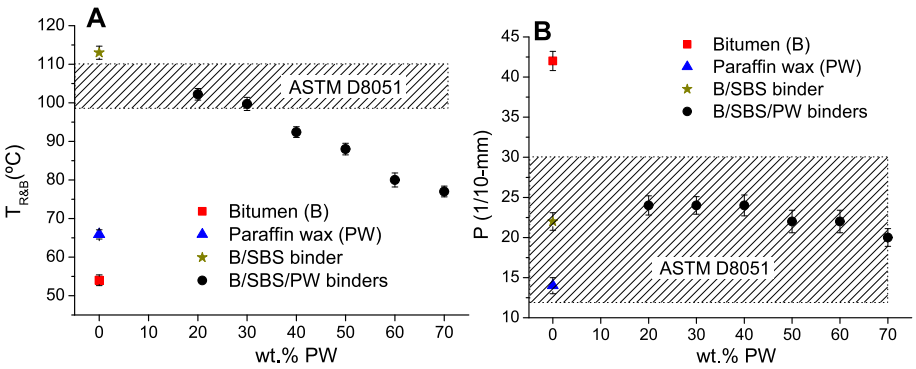

Fig. 5. Effect of PW concentration on A) ring and ball softening temperature and B) penetration values for ternary B/SBS/PW blends.

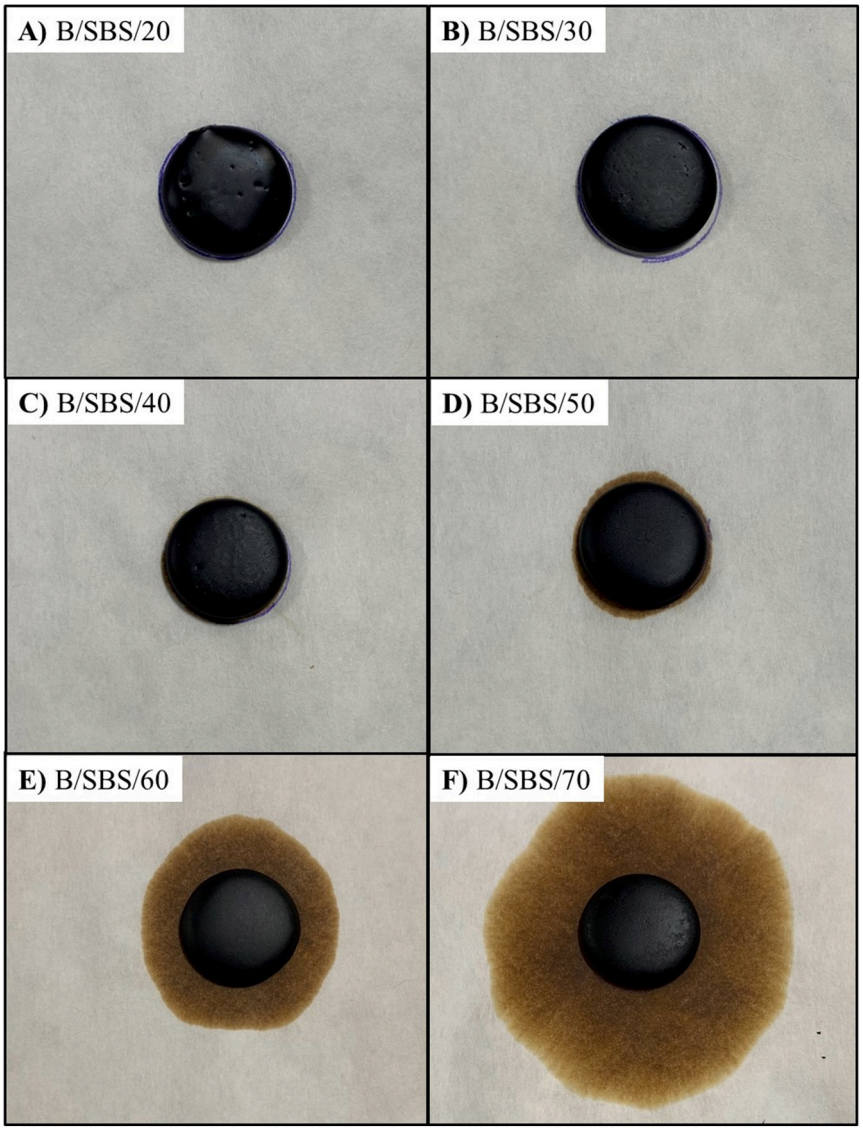

Fig. 6. Digital photographs of ternary B/SBS/PW blends after leakage test.

that they could migrate to the paraffin-rich phase, leading to morphological changes in the PW phase [35]. Anyway, the melting/crystallization temperatures reported for the ternary blends are within the specific temperature range for solar energy applications [30].

For being applied as roofing materials, the ternary blends here proposed must exhibit suitable thermal storage capacity after a long-term utility period and be able to resist cyclic repeated melting and crystallization cycles. To that end, a thermal cycling test was conducted on the selected ternary blends to explore their thermal reliability. Fig. 7B portrays DSC curves for B/SBS/20 and B/SBS/30 binder after 50 thermal cycling, and their corresponding thermal characteristics are also gathered in Table 2. Interestingly, negligible changes in the melting and

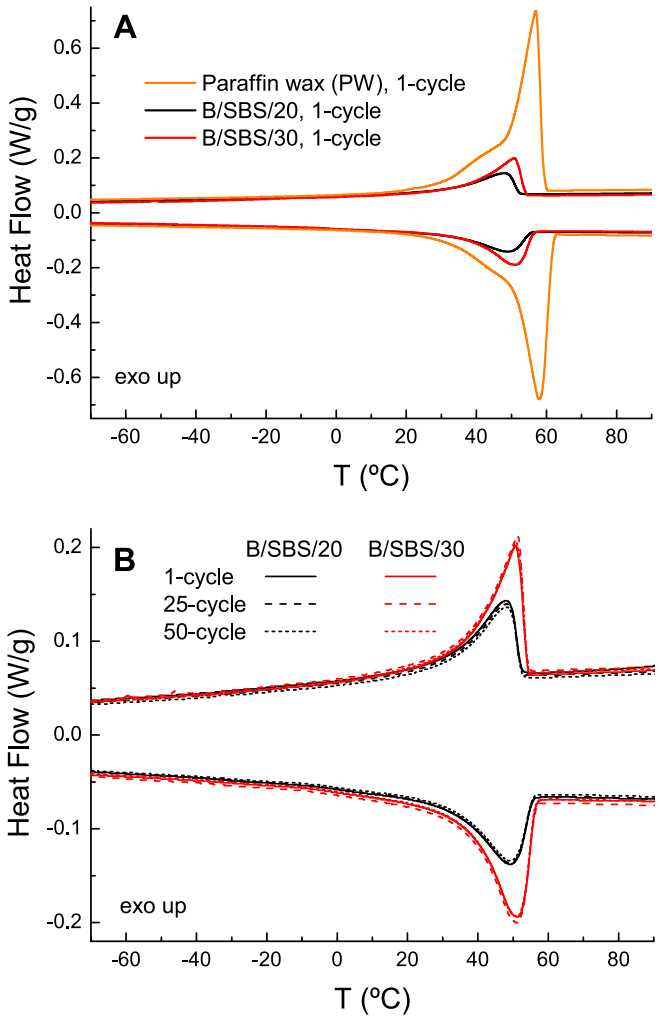

Fig. 7. DSC scans for pristine PW and selected ternary binders.

crystallization curves are noticed on both binders after thermal cycling, which results in nearly coincident values of characteristic temperatures and enthalpies. Therefore, these results indicate that both ternary blends can maintain good thermal cycling reliability after long-term utility period.

Furthermore, the crystallinity degree (χ, which is calculated from the melting enthalpy divided by the melting enthalpy of perfectly crystalline polyethylene (293 J/g) [33] and by the PW mass fraction) provide valuable information. While pristine PW presents 73.7 % crystallinity, this value is reduced to ca. 71.5 and 67.7 % for ternary blends when PW concentration is increased up to 20 and 30 wt%, respectively. These results indicate that most of the crystalline structure of PW is retained in the ternary blends and that the other portion is solubilized in the bitumen. This last portion together with the amorphous PW phase would increase the proportion of light compounds in the bitumen and explain the above-commented improvement in the low-temperature flexibility of the ternary blends. It is worth mentioning that the crystallinity degree of ternary blends, especially for that containing 30 wt% PW, is not reduced in a large extent, which means a large capacity to store thermal energy. In fact, the phase change enthalpy of B/SBS/30 binder (ca. 60 J/g) is in line with other efficient energy building materials based on PCMs [36].

Moreover, the relative enthalpy efficiency (λ) can be also calculated by the following formula [37]:

$$\lambda = \frac{\Delta H_{m,blend}}{\Delta H_{m,PW} \times w_{PW}} \times 100 \quad (2)$$

where $\Delta H_{m,blend}$ is the melting enthalpy of ternary B/SBS/PW blends, $\Delta H_{m,PW}$ is the melting enthalpy of pristine paraffin wax, and w_{PW} corresponds to the weight content of paraffin wax in the blend. This parameter gives information about the latent heat loss of PW in the ternary blends. Interestingly, as seen in Table 2, B/SBS/20 and B/SBS/30 binders present λ values of ca. 97 % and 92 %, respectively. These results indicate that the latent heat capacity of PW is slightly reduced in the ternary B/SBS/PW blends, which are in line with the conclusions derived from the crystallinity degrees.

3.2.2. *Thermal conductivity and specific heat capacity*

In addition to thermal storage capacity and thermal reliability, efficient phase change materials should exhibit other favourable thermal properties that enhance the thermal energy storage. A crucial factor in assessing the performance of these materials is their thermal conductivity, which has a direct impact on how effectively them transfer heat. Thus, low thermal conductivity values will reduce the rate of storage and release heat during melting and freezing processes. To study this, Fig. 8A shows the in-plane thermal conductivity (k) of pristine paraffin wax (PW), bitumen (B), reference binary blend (B/SBS) and the selected ternary binders as a function of testing temperature. On the one hand, in-plane thermal conductivities hardy change for B with temperature, displaying the lowest values; similar trend is also observed for the B/SBS binder, but with slightly higher values, likely, due to the SBS addition. On the other hand, PW shows higher and constant conductivities until the onset of its melting process ($T_{m,o}$, gathered in Table 2), followed by an noticeable drop. Ternary B/SBS/PW binders show a similar pattern, but with less pronounced drops starting at lower temperatures (in good agreement with their lower $T_{m,o}$ values). As expected, B/SBS/30 sample shows higher in-plane thermal conductivities than S/SBS/20, which would enhance the efficiency of the thermal energy storage by reducing the time needed for the heat charging/discharging processes.

Interesting results can be also derived from the relationship between specific heat capacity (C_p) and testing temperature for the different samples shown in Fig. 8B. Whereas specific heat capacity of reference binary B/SBS sample slightly increases with testing temperature, pristine PW displays a remarkable asymmetric peak centred at 58 °C (which corresponds to its maximum melting temperature, $T_{m,p}$, in Table 2). The presence of this event is also noticed on the ternary blends, especially for that containing 30 wt% PW. Therefore, in the range 30–60 °C at which

Table 2
Thermal characteristics of PW and the selected ternary binders after 1, 25 and 50 thermal cycles.

		Crystallization			Melting				
		ΔH_c (J/g)	$T_{c,o}$ (°C)	$T_{c,p}$ (°C)	ΔH_m (J/g)	$T_{m,o}$ (°C)	$T_{m,p}$ (°C)	χ (%)	λ (%)
	PW	215.55 ± 0.9	59.2 ± 0.2	56.9 ± 0.4	215.95 ± 0.6	49.0 ± 0.2	57.9 ± 0.5	73.7 ± 0.4	–
B/SBS/20	1-cycle	41.56 ± 0.7	52.3 ± 0.5	48.1 ± 0.8	41.80 ± 0.3	30.9 ± 0.3	49.1 ± 0.6	71.3 ± 0.3	96.8 ± 0.3
	25-cycle	41.14 ± 0.6	52.2 ± 0.5	48.0 ± 0.4	42.02 ± 0.2	31.0 ± 0.2	49.2 ± 0.4	71.7 ± 0.5	97.3 ± 0.4
	50-cycle	41.66 ± 0.5	52.3 ± 0.4	48.1 ± 0.7	41.87 ± 0.4	30.9 ± 0.3	49.1 ± 0.6	71.4 ± 0.4	96.9 ± 0.3
B/SBS/30	1-cycle	60.65 ± 0.9	53.9 ± 0.6	50.7 ± 0.5	59.56 ± 0.6	37.0 ± 0.4	51.2 ± 0.5	67.8 ± 0.4	91.9 ± 0.4
	25-cycle	60.76 ± 0.8	53.9 ± 0.6	51.2 ± 0.5	59.50 ± 0.4	36.9 ± 0.5	50.9 ± 0.6	67.7 ± 0.3	91.8 ± 0.3
	50-cycle	60.16 ± 0.7	54.0 ± 0.5	50.9 ± 0.6	59.70 ± 0.6	37.0 ± 0.5	51.1 ± 0.6	67.9 ± 0.5	92.2 ± 0.6

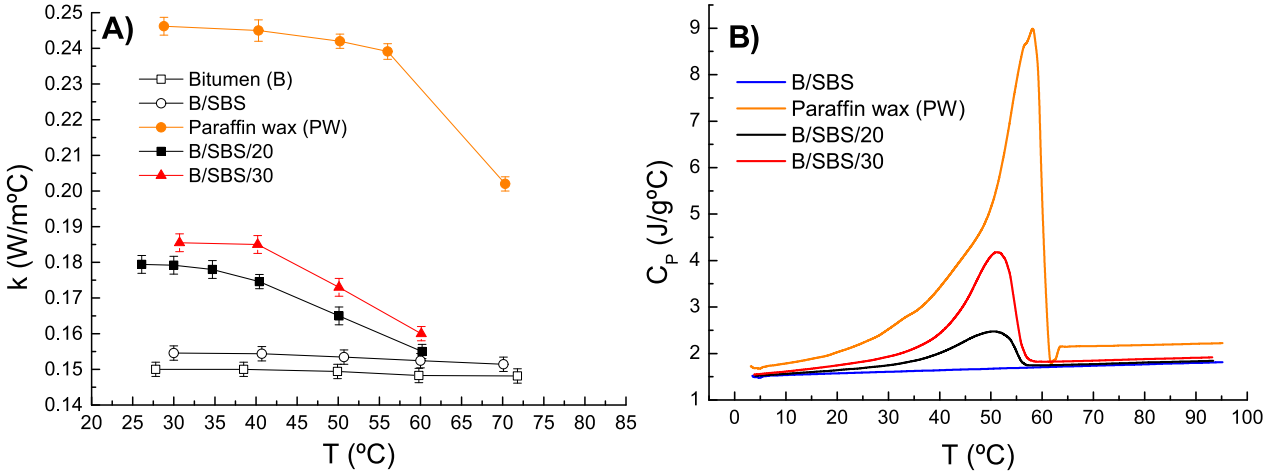

Fig. 8. Evolution of A) in-plane thermal conductivity and B) specific heat capacity with testing temperature for different samples.

the thermoregulation effect for solar energy application is considered, the higher specific heat capacities of B/SBS/30 binder compared to reference B/SBS sample would contribute to a good temperature regulation ability [38].

3.2.3. *Temperature regulation performance*

The temperature regulation performance of the selected ternary binders compared to the reference binary sample was studied following the experimental setup described in the Supporting Information. The test consisted of two consecutive stages of 30 min each: i) firstly, sample was subjected to the action of a simulated solar irradiation at a constant radiant flux density ($q^* = 1460$ W/m^2 at the sample centre); and ii) then, the solar lamp was turned off (and, thereby, $q^* = 0$ W/m^2). To ensure that all PW in the ternary blends melts, the sink temperature (T_S) was set a 32.0 °C for all tests, which is close to the onset of the melting temperature ($T_{m,o}$ in Table 2) for B/SBS/20 sample. Thus, by selecting $T_{ambient} = 25$ °C, $T_S = 32.0$ °C and $q^* = 1460$ W/m^2, the sample temperature at the bottom and top take values of ca. 32 °C and 60 °C, respectively. Fig. 9 shows the temperature-time curve of the top surface (T_0), and the temperature at 2.2 mm (T_1), 3.4 mm (T_2) and 6.8 mm (T_3) depth to sample surface for the different binders.

During the first stage, the irradiation received on the top surface of the sample is partially absorbed (and the heat is conducted through the material), and the rest is reflected, emitted as heat radiation and lost by free convection [39]. As can be observed, each temperature displays a temperature-time profile characterized by a rapid increase until the steady state (or equilibrium) is reached. As expected, for each sample, the steady state temperatures (T_{SS}) decrease with increasing the distance from the top (or depth). The thermoregulation ability of ternary B/SBS/PW binders is clearly noted by comparing their heating curves with those for the binary B/SBS sample (without PW). In this first stage, the testing temperature reached the phase change temperature, and the PW inside of the ternary blends started melting to absorb solar-thermal energy and stored it in the way of latent heat [40]. This fact is reflected in lower initial heating rates for the ternary blends compared to the binary B/SBS binder.

The steady state temperatures (T_{SS}) can be also used to calculate a local heat flux transferred by a conduction mechanism at the sample centre for each sample, q_c, by means of the Fourier's law (Eq. (3)):

$$q_c = -k\frac{dT}{dx} \tag{3}$$

where k is the average material in-plane thermal conductivity (gathered in Fig. 8A) within the T_{SS} range and x is related to the depth to surface of each temperature sensor. The evolution of T_{SS} with sensor depth for each sample is illustrated in Fig. 10.

The local heat flux conducted through sample centre (q_c) can be calculated from the linear fitting from Fig. 10 (this is, $-q_c/k$), and

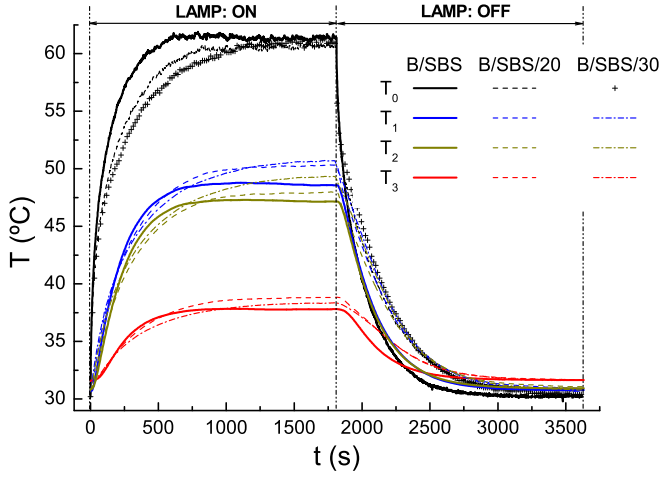

Fig. 9. Temperature-time curve of the different temperature sensors (see Fig. S1 in the Supporting Information) for reference binary B/SBS sample and selected B/SBS/PW binders.

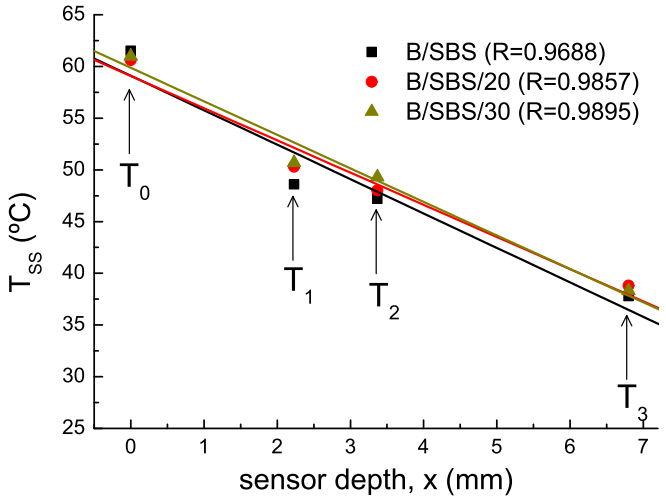

Fig. 10. Steady state temperatures (T_{SS}) as a function of sensor depth for reference binary B/SBS sample and selected B/SBS/PW binders.

compared with the solar irradiation flux at the sample centre supplied by the solar lamp ($q^* = 1460$ W/m^2) to determinate the material capability of solar heat absorption, q_{abs}, as follows:

$$q_{abs} = \frac{q_c}{q^*} \times 100 \quad (4)$$

For the selected test conditions ($T_{ambient} = 25$ °C, $T_s = 32$ °C and $q^* = 1460$ W/m^2), a similar value of solar heat absorption capability (ca. 35.5 %) is calculated for B/SBS and B/SBS/20 binder; however, this value increases up to 38.4 % for the ternary B/SBS/30 sample. Although initially this fact could imply a higher heat conducted through the B/SBS/30 binder into the building, which might be undesirable depending on weather conditions, this is largely counteracted by its great thermoregulation ability.

Finally, the cooling curves of the second stage (marked as "LAMP: OFF" in Fig. 9) can be used to quantify the thermoregulation effect noticed on ternary blends. In this stage, the thermoregulation ability of ternary blends compared to binary B/SBS sample is detected by higher temperatures during the cooling process and lower cooling rates. The dampening of the temperature drop is a consequence of the heat released in the course of the PW crystallization. This can be clearly visualized in Fig. 11, in which the temperature differences between each ternary blend and reference B/SBS sample ($\Delta T = T_{B/SBS/PW}$-$T_{B/SBS}$) are plotted versus the time elapsed after switching off the lamp.

Thus, after a few seconds without irradiation, a continuous increase in ΔT curves related to the initiation of thermoregulation effect is observed. Then, ΔT curves reach a maximum and, subsequently, decrease and tend to stabilize. From Fig. 11, a Latent Heat Thermoregulation Index (LHTI) can be calculated according to that reported by Ma et al. [18]:

$$LHTI = \frac{\int_{t_0}^{t_{max}} \Delta T \, dt}{(t_{max} - t_0) \times \left(\Delta T|_{t_{max}} - \Delta T|_{t_0}\right)} \quad (5)$$

where t_0 and $\Delta T|_{t_0}$ are the time and ΔT value when thermoregulation effect begins; and t_{max} and $\Delta T|_{t_{max}}$ the time and ΔT value at which the maximum is reached. Thus, whereas $\int_{t_0}^{t_{max}} \Delta T \, dt$ indicates the thermal regulation ability of a PCM with the accumulation of temperature difference in a certain time range, LHTI reflects the efficiency of latent heat thermoregulation [18]. An average LHTI value of 0.85 ± 0.19 was calculated for B/SBS/20 binder, increasing up to 1.22 ± 0.15 for B/SBS/30 sample. Even though LHTI values depend on the temperature cooling rate applied in the temperature-regulation test [19], the values here obtained are higher than those previously reported for bitumen modified with a 6 wt% microencapsulated PEG-2000 [19] or 7 wt% polyurethane solid-solid phase change material [41]. Therefore, these findings demonstrate that the selected ternary B/SBS/PW binders, particularly B/SBS/30, may be considered roofing materials with promising potential for efficient energy storage applications.

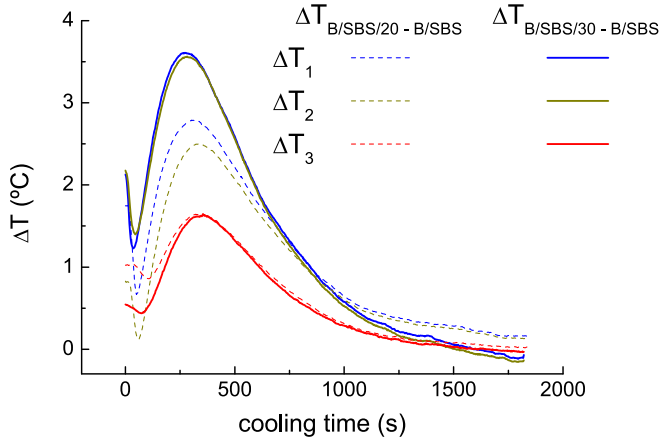

Fig. 11. Temperature differences between each ternary blend and reference B/SBS sample ($\Delta T = T_{B/SBS/PW}$-$T_{B/SBS}$) recorded at positions 1 to 3, as a function of the elapsed time after switching off the lamp.

4. Concluding remarks

Form-stable bitumen/paraffin-wax/SBS binders were successfully manufactured to be applied as energy-efficient building materials with advanced thermal energy storage and thermoregulation features. The creation of a well-developed SBS/bitumen matrix is a feasible procedure to enclose PCM that may prevent its leakage, unlike more complex alternatives such as PCM microencapsulation or the use of inorganic porous materials. Firstly, the effects of paraffin wax concentration on microstructure, thermal stability, rheological properties, technological tests and leakproof performance of ternary blends (formulated at a fixed B/SBS mass ratio) were evaluated. All roofing materials show excellent thermal stability regardless of PW concentration, and the rheological properties (low-temperature flexibility, structural integrity at 30 °C and binder elastic properties) improve as PW content in ternary blends increases. However, the softening temperature requirements, specified by ASTM D8051 for wax-modified asphaltic roofing products, limited the maximum PW concentration to 30 wt%. Interestingly, no liquid PCM leakage was detected for the ternary blends formulated with up to 30 wt % PW. Conversely, PW leakage was massive for ternary blends with ring and ball softening temperature lower than 80 °C (temperature used in the leakage test). Under such conditions, the created SBS network collapses and, thereby, the PW leakage is favoured. Selected ternary blends (B/SBS/20 and B/SBS/30) were subjected to a comprehensive thermal and solar assessment. Both prototypes exhibited great thermal cycling reliability after long-term utility period, and the thermal storage capacity (with a phase change enthalpy of ca. 60 J/g for B/SBS/30, located at ca. 30–55 °C), is in line with other efficient energy building materials based on PCMs. In addition, thermal properties like thermal conductivity and specific heat capacity indicate a good thermoregulation ability. In fact, the temperature regulation tests (by using a simulated solar irradiation) conducted on prototypes, yield Latent Heat Thermoregulation Index values of roofing materials with promising potential for efficient energy storage/thermoregulation applications.

Funding

This work is part of the project TED2021-131284B-I00 funded by MCIN/AEI/10.13039/501100011033 (Spanish Ministry of Science and Innovation) and European Union Next Generation EU/PRTR; and the Cátedra Fundación CEPSA through the project "BituFoil" of the edition 2023. Clara Delgado-Sánchez also acknowledges financial support from Junta de Andalucía through post-doctoral Grant No. DC 01228 (PAIDI 2020), co-funded by the EU Fondo Social Europeo (FSE). Funding for open access charge: Universidad de Huelva / CBUA.

CRediT authorship contribution statement

A.A. Cuadri: Writing – review & editing, Writing – original draft, Project administration, Methodology, Investigation, Funding acquisition, Formal analysis, Conceptualization. **C. Delgado-Sánchez:** Investigation, Formal analysis. **A. Tenorio-Alfonso:** Investigation, Formal analysis. **P. Partal:** Writing – review & editing, Writing – original draft, Methodology, Formal analysis, Conceptualization. **F.J. Navarro:** Writing – review & editing, Project administration, Methodology, Funding acquisition.

Declaration of competing interest

The authors declare that they have no known competing financial

interests or personal relationships that could have appeared to influence the work reported in this paper.

Data availability

The authors do not have permission to share data.

Appendix A. Supplementary data

Supplementary data to this article can be found online at https://doi.org/10.1016/j.est.2024.112420.

References

[1] T. Khadiran, M.Z. Hussein, Z. Zainal, R. Rusli, Shape-stabilised n-octadecane/activated carbon nanocomposite phase change material for thermal energy storage, J. Taiwan Inst. Chem. Eng. 55 (2015) 189–197, https://doi.org/10.1016/j.jtice.2015.03.028.

[2] C. Alkan, E.H. Alakara, S.A. Aksoy, I. Demir I, Cement mortar composites including 1-tetradecanol@PMMA Pickering emulsion particles for thermal energy management of buildings, Chem. Eng. J. 476 (2023) 146843, https://doi.org/10.1016/j.cej.2023.146843.

[3] X. Yao, Y. Chen, H. Gu, J. Gou, D. Zou, Preparation and thermophysical properties of a novel metallic microencapsulated phase change material/eutectic salt/ceramic composite, Chem. Eng. J. 477 (2023) 146967, https://doi.org/10.1016/j.cej.2023.146967.

[4] D. Zhou, Y. Tian, Review on thermal energy storage with phase change materials (PCMs) in building applications, Appl. Energy 92 (2012) 593–605, https://doi.org/10.1016/j. apenergy.2011.08.025.

[5] A. Ismail, J. Wang, B.A. Salami, L.O. Oyedele, G.K. Otukogbe, Microencapsulated phase change materials for enhanced thermal energy storage performance in construc- tion materials: a critical review, Constr. Build. Mater. 401 (2023) 132877, https://doi.org/10.1016/j.conbuildmat.2023.132877.

[6] Y. Chen, H. Wang, Z. You, N. Hossiney, Application of phase change material in asphalt mixture – a review, Constr. Build. Mater. 263 (2020) 120219, https://doi.org/10.1016/j. conbuildmat.2020.120219.

[7] F.J. Ortega, F.J. Navarro, M. García-Morales, T. McNally, Thermo-mechanical behaviour and structure of novel bitumen/nanoclay/MDI composites, Compos. Pt. B-Eng. 76 (2015) 192–200, https://doi.org/10.1016/j.compositesb.2015.02.030.

[8] G. Polacco, J. Stastna, D. Biondi, L. Zanzotto, Relation between polymer architecture and nonlinear viscoelastic behavior of modified asphalts, Curr. Opin. Colloid Interface Sci. 245 (2006) 11230, https://doi.org/10.1016/j.cocis.2006.09.001.

[9] M. Jia, A. Sha, W. Jiang, X. Li, W. Jiao, Developing a solid–solid phase change heat storage asphalt pavement material and its application as functional filler for cooling asphalt pavement, Energ. Buildings 285 (2023) 112935, https://doi.org/10.1016/j.enbuild.2023.11 2935.

[10] Y. Lou, Y. Xie, H. Jiang, Y. Chen, L. Zhang, X. Sheng, D. Xie, H. Wu, Y. Mei, Flame-retardant and form-stable phase change composites based on MXene with high thermostability and thermal conductivity for thermal energy storage, Chem. Eng. J. 420 (2021) 130466, https://doi.org/10.1016/j.cej.2021.130466.

[11] T. Ma, L. Li, Q. Wang, C. Guo, High-performance flame retarded paraffin/epoxy resin form-stable phase change material, J. Mater. Sci. 54 (2019) 875–885, https://doi.org/10.1007/s10853-018-2846-7.

[12] L. Xu, X. Liu, R. Yang, Flame retardant paraffin-based shape-stabilized phase change material via expandable graphite-based flame-retardant coating, Molecules 25 (2020) 2408, https://doi.org/10.3390/molecules25102408.

[13] R.u. Zhou, Z. Ming, J. He, Y. Ding, J. Jiang, Effect of magnesium hydroxide and aluminum hydroxide on the thermal stability, latent heat and flammability properties of paraffin/HDPE phase change blends, Polymers 12 (2020) 180, https://doi.org/10.3390/polym12010180.

[14] Y. Cai, Y. Hu, L. Song, Q. Kong, R. Yang, Y. Zhang, Z. Chen, W. Fan, Preparation and flammability of high density polyethylene/paraffin/organophilic montmorillonite hybrids as a form stable phase change material, Energy Convers. Manag. 48 (2007) 462–469, https://doi.org/10.1016/j.enconman.2006.06.021.

[15] M.M. Velencoso, A. Battig, J.C. Markwart, B. Schartel, F.R. Wurm, Molecular firefighting—how modern phosphorus chemistry can help solve the challenge of flame retardancy, Angew. Chem. Int. Ed. 57 (2018) 10450–10467, https://doi.org/10.1002/anie.201711735.

[16] U. Braun, A.I. Balabanovich, B. Schartel, U. Knoll, J. Artner, M. Ciesielski, M. Döring, R. Perez, J.K.W. Sandler, V. Altstadt, T. Hoffmann, D. Pospiech, Influence of the oxidation state of phosphorus on the decomposition and fire behaviour of flame-retarded epoxy resin composites, Polymer 47 (2006) 8495–8508, https://doi.org/10.1016/j.polymer.2006.10.022.

[17] M.R. Kakar, Z. Refaa, J. Worlitsfheck, A. Stamatiou, M.N. Partl, M. Bueno, Thermal and rheological characterization of bitumen modified with microencapsulated phase change materials, Constr. Build. Mater. 215 (2019) 171–179, https://doi.org/10.1016/j. conbuildmat.2019.04.171.

[18] B. Ma, S.S. Chen, K. Wei, F.W. Liu, X.Y. Zhou, Analysis of thermoregulation indices on microencapsulated phase change materials for asphalt pavement, Constr. Build. Mater. 208 (2019) 402–412, https://doi.org/10.1016/j.conbuildmat.2019.03.014.

[19] S. Wang, K. Wei, W. Shi, P. Cheng, J. Shi, B. Ma, Study on the rheological properties and phase-change temperature regulation of asphalt modified by high/low-temperature phase change material particles, J. Energy Storage 56 (2022) 105970, https://doi.org/10.1016/j.est.2022.105970.

[20] M.R. Kakar, Z. Refaa, J. Worlitschek, A. Stamatiou, M.N. Partl, M. Bueno, Effects of aging on asphalt binders modified with microencapsulated phase change material, Compos. Pt. B-Eng. 173 (2019) 107007, https://doi.org/10.1016/j.compositesb.2019.107007.

[21] H.M. Ali, T. Rehman, M. Arıcı, Z. Said, B. Durakovic, H.I. Mohammed, R. Kumar, M.K. Rathod, O. Buyukdagli, M. Teggar, Advances in thermal energy storage: fundamentals and applications, Prog. Energy Combust. Sci. 100 (2024) 101109, https://doi.org/10.1016/j.pecs.2023.101109.

[22] X. Huang, X. Chen, A. Li, D. Atinafu, H. Gao, W. Dong, G. Wang, Shape-stabilized phase change materials based on porous supports for thermal energy storage applications, Chem. Eng. J. 356 (2019) 641–661, https://doi.org/10.1016/j.cej.2018.09.013.

[23] M. Hu, D. Wang, G. Kokogiannakis, J. Darkwa, Y. Li, L. Wang, Q. Xu, W. Su, Enhancement of thermal and mechanical properties of microencapsulated phase change materials with graphene oxide, Chem. Eng. J. 479 (2024) 147855, https://doi.org/10.1016/j.cej. 2023.147855.

[24] S. Yu, S.W. Jeong, O. Chung, S. Kim, Bio-based PCM/carbon nanomaterials composites with enhanced thermal conductivity, Sol. Energy Mater. Sol. Cells 120 (2014) 549–554, https://doi.org/10.1016/j.solmat.2013.09.037.

[25] B. Ma, W. Si, J. Ren, H.N. Wang, F.W. Liu, J. Li, Exploration of road temperature-adjustment material in asphalt mixture, Road Mater. Pavement Des. 15 (2014) 659–673, https://doi.org/10.1080/14680629.2014.885462.

[26] G.D. Airey, Rheological properties of styrene butadiene styrene polymer modified road bitumens, Fuel 82 (2003) 1709–1719, https://doi.org/10.1016/S0016-2361(03)00146-7.

[27] M.J. Martín-Alfonso, P. Partal, F.J. Navarro, M. García-Morales, C. Gallegos, Use of MDI-functionalized reactive polymer for the manufacture of modified bitumen with enhanced properties for roofing applications, Eur. Polym. J. 44 (2008) 1451–1461, https://doi.org/10.1016/j.eurpolymj.2008.02.026.

[28] Y. Su, S. Tang, M. Cai, Y. Nie, B. Hu, S. Wu, C. Cheng, Thermal oxidative aging mechanism of lignin modified bitumen, Constr. Build. Mater. 363 (2023) 129863, https://doi.org/10.1016/j.conbuildmat.2022.129863.

[29] M.J. Martín-Alfonso, P. Partal, F.J. Navarro, M. García-Morales, C. Gallegos, Role of water in the development of new isocyanate-based bituminous products, Ind. Eng. Chem. Res. 47 (2008) 6933–6940, https://doi.org/10.1021/ie800243w.

[30] K. Du, J. Calautit, Z. Wang, Y. Wu, H. Liu, A review of the applications of phase change materials in cooling, heating and power generation in different temperature ranges, Appl. Energy 220 (2018) 242–273, https://doi.org/10.1016/j.apenergy.2018.03.005.

[31] K.Y. Leong, S. Hasbi, K.Z.K. Ahmad, N.M. Jali, H.C. Ong, M.F.M. Din, Thermal properties evaluation of paraffin wax enhanced with carbon nanotubes as latent heat thermal energy storage, J. Energy Storage 52 (2022) 105027, https://doi.org/10.1016/j.est.2022.105027.

[32] W. Kong, Z. Liu, Y. Yang, C. Zhou, J. Lei, Preparation and characterizations of asphalt/lauric acid blends phase change materials for potential building materials, Constr. Build. Mater. 152 (2017) 568–575, https://doi.org/10.1016/j.conbuildmat.2017.05.039.

[33] C. Gutiérrez-Blandón, A.A. Cuadri, A. Tenorio-Alfonso, P. Partal, F.J. Navarro, Rheological and phase behaviour of paraffin wax/bitumen blends with thermal storage characteristics, Constr. Build. Mater. 401 (2023) 132826, https://doi.org/10.1016/j.conbuildmat. 2023.132826.

[34] O.V. Laukkanen, H. Soenen, H.H. Winter, J. Seppälä, Low-temperature rheological and morphological characterization of SBS modified bitumen, Constr. Build. Mater. 179 (2018) 348–359, https://doi.org/10.1016/j.conbuildmat.2018.05.160.

[35] I.N. Frolov, E.S. Okhotnikova, M.A. Ziganshin, A.A. Firsin, Cold crystallization event on DSC heating curves of bitumen, J. Therm. Anal. Calorim. 147 (2022) 5269–5278, https://doi.org/10.1007/s10973-021-10908-x.

[36] C. Fabiani, A.L. Pisello, M. Barbanera, L.F. Cabeza, Palm oil-based bio-PCM for energy efficient building applications: multipurpose thermal investigation and life cycle assessment, J. Energy Storage 28 (2020) 101129, https://doi.org/10.1016/j.est.2019.101129.

[37] X. Liu, J. Huang, W.Y. Wong, J. Qu, A novel-based polyurethane/wood powder composite as shape-stable phase change material with high relative enthalpy efficiency for solar thermal energy storage, Sol. Energy Mater. Sol. Cells 200 (2019) 109987, https://doi.org/10.1016/j.solmat.2019.109987.

[38] Z. Liu, K. Wei, S. Wang, B. Ma, X. Wang, W. Shi, J. Xu, Effect of high-temperature-resistant epoxy resin/polyethylene glycol 2000 composite stereotyped phase change material particles on asphalt properties, Constr. Build. Mater. 300 (2021) 124007, https://doi.org/10.1016/j.conbuildmat.2021.124007.

[39] R. Álvarez-Barajas, A.A. Cuadri, C. Delgado-Sánchez, F.J. Navarro, P. Partal, Non-bituminous binders formulated with bio-based and recycled materials for energy-efficient roofing applications, J. Clean. Prod. 393 (2023) 136350, https://doi.org/10.1016/j.jclepro.2023.136350.

[40] J. Huang, Y. Liu, J. Lin, J. Su, C. Redshaw, X. Feng, Y. Min, Novel pyrene-based aggregation-induced emission luminogen (AIEgen) composite phase change fibers with satisfactory fluorescence anti-counterfeiting, temperature sensing, and high-temperature warning functions for solar-thermal energy storage, Adv. Compos. Hydrid Mater. 6 (2023) 126, https://doi.org/10.1007/s42114-023-00706-4.

[41] K. Wei, X. Wang, B. Ma, W. Shi, S. Duan, F. Liu, Study on rheological properties and phase-change temperature control of asphalt modified by polyurethane solid–solid phase change material, Sol. Energy 194 (2019) 893–902, https://doi.org/10.1016/j.solener.2019.11.007.